Dynamical stability indicator based on autoregressive moving-average models: Critical transitions and the Atlantic meridional overturning circulation

iD **Marie Rodal,** iD **Sebastian Krumscheid,** iD **Gaurav Madan, et al.**

COLLECTIONS

Paper published as part of the special topic on Theory-informed and Data-driven Approaches to Advance Climate Sciences

View Online   Export Citation   CrossMark

ARTICLES YOU MAY BE INTERESTED IN

Transition from inhomogeneous limit cycles to oscillation death in nonlinear oscillators with similarity-dependent coupling
Chaos: An Interdisciplinary Journal of Nonlinear Science **32**, 113138 (2022); https://doi.org/10.1063/5.0100595

A data-driven approach for discovering the most probable transition pathway for a stochastic carbon cycle system
Chaos: An Interdisciplinary Journal of Nonlinear Science **32**, 113140 (2022); https://doi.org/10.1063/5.0116643

Giant oscillations of diffusion in ac-driven periodic systems
Chaos: An Interdisciplinary Journal of Nonlinear Science **32**, 113106 (2022); https://doi.org/10.1063/5.0117902
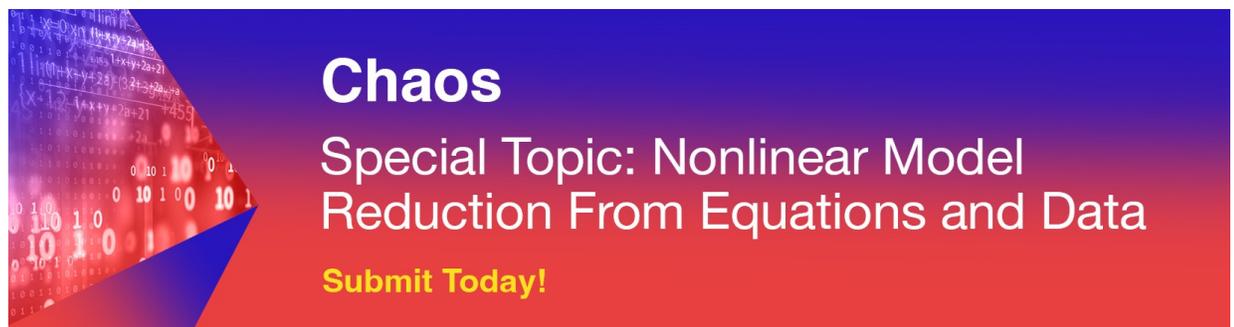
Chaos

Special Topic: Nonlinear Model Reduction From Equations and Data

Submit Today!

Dynamical stability indicator based on autoregressive moving-average models: Critical transitions and the Atlantic meridional overturning circulation

Marie Rodal,[1,2,a] (ID) Sebastian Krumscheid,[3] (ID) Gaurav Madan,[4] (ID) Joseph Henry LaCasce,[4] (ID) and Nikki Vercauteren[4,b] (ID)

AFFILIATIONS

[1] FB Mathematik und Informatik, Freie Universität Berlin, Arnimallee 6, 14195 Berlin, Germany
[2] University of Antwerp, Department of Biology, PLECO, Campus Drie Eiken - D.C.013, Universiteitsplein 1 BE-2610 Wilrijk, Belgium
[3] Karlsruhe Institute of Technology, 76131 Karlsruhe, Germany
[4] Section for Meteorology and Oceanography, Department of Geosciences, University of Oslo, Blindernveien 31, Kristine Bonnevies hus, 0371 Oslo, Norway

Note: This article is part of the Focus Issue, Theory-informed and Data-driven Approaches to Advance Climate Sciences.
[a] **Author to whom correspondence should be addressed:** marie.rodal@uantwerpen.be
[b] nikki.vercauteren@geo.uio.no

ABSTRACT

A statistical indicator for dynamic stability, known as the Υ indicator, is used to gauge the stability and, hence, detect approaching tipping points of simulation data from a reduced five-box model of the North Atlantic Meridional Overturning Circulation (AMOC) exposed to a time-dependent hosing function. The hosing function simulates the influx of fresh water due to the melting of the Greenland ice sheet and increased precipitation in the North Atlantic. The Υ indicator is designed to detect changes in the memory properties of the dynamics and is based on fitting auto-regressive moving-average models in a sliding window approach to time series data. An increase in memory properties is interpreted as a sign of dynamical instability. The performance of the indicator is tested on time series subject to different types of tipping, namely, bifurcation-induced, noise-induced, and rate-induced tipping. The numerical analysis shows that the indicator indeed responds to the different types of induced instabilities. Finally, the indicator is applied to two AMOC time series from a full complexity Earth systems model (CESM2). Compared with the doubling CO_2 scenario, the quadrupling CO_2 scenario results in stronger dynamical instability of the AMOC during its weakening phase.

Published under an exclusive license by AIP Publishing. https://doi.org/10.1063/5.0089694

A statistical indicator for dynamic stability is applied to simulation data from an ocean circulation model. The indicator assesses the stability of the time series data and gives indication of approaching tipping points. Three different types of tipping, defined by their causing mechanism, are explored. In addition, the indicator's reaction to the application of colored, as opposed to white, noise is assessed. Finally, the indicator is compared to other statistical early-warning indicators.

I. INTRODUCTION

Tipping points, or critical transitions, are sudden, drastic changes in a system resulting from initial small perturbations. The study of tipping points is of particular interest to climate scientists and ecologists, as several theoretical studies highlight such tipping for an assortment of climatic and ecological systems, and observations also indicate that abrupt changes are, indeed, common in nature.[1]

Ashwin et al.[2] classified tipping points according to the causing mechanism, yielding three classes of tipping points. Bifurcation-induced tipping, or B-tipping, occurs when a steady change in a parameter past a threshold induces a sudden qualitative change in the system's behavior. Noise-induced tipping, or N-tipping, occurs when short-timescale internal variability causes the system to transition between different co-existing attracting states. Finally, rate-induced tipping, or R-tipping, occurs when the system fails to track a continuously changing attractor and, hence, abruptly leaves the attractor.

Of these three, rate-induced tipping is certainly the least studied; however, as demonstrated by Scheffer et al.,[3] Wieczorek et al.,[4] and, more recently, O'Keeffe and Wieczorek,[5] it is an important tipping mechanism that cannot be explained through classical bifurcation theory. Indeed, when the system is unable to track a continuously available quasi-stable state due to the system parameters changing too quickly, it might shift to another available equilibrium state without crossing a bifurcation boundary. There are a few methods available for estimating what exactly "too quickly" means; see Wieczorek and Perrymann,[6] Ashwin et al.,[7] Vanselow et al.,[8] and OKeeffe and Wieczorek,[5] but they depend strongly on the time-dependent parameter function, in particular, its asymptotic properties. Finding generalizable methods for determining the rate of the parameter drift that induces tipping will be of great interest going forward. Another issue of great practical importance is the question of how to obtain early warnings for such tipping points, in particular, if classical methods for stability analysis also remain valid in the regime of rapid parameter changes.

Ritchie and Sieber[9] showed that for rate-induced tipping, the most commonly used early-warning indicators, namely, an increase in variance and an increase in autocorrelation, occur not when the equilibrium drift is the fastest but with a delay. This suggests that these indicators might not be able to detect tipping before it has already occurred, although their analysis does give indication that the theory behind these indicators, the so-called critical slowing down, may still hold for rate-induced tipping.

In this paper, we study an indicator for dynamic stability, from now on referred to as the Υ indicator, initially proposed by Faranda et al.[10] The Υ indicator uses auto-regressive moving-average or ARMA(p,q) models to estimate how close a system is to an equilibrium. It is based on the observation that the dynamics of an observable arising from a potentially complex system very close to a stable equilibrium will appear like a random walk with a tendency to be attracted to a well-defined equilibrium. When discretized, such dynamics can be well represented by an ARMA(1,0) process. When approaching a transition, however, the system may experience critical slowing down and diverging memory properties. The trajectory of the observable, hence, experiences new timescales, which can be detected even with a limited dataset through an increase in the necessary memory lags of fitted ARMA(p,q) models.[11] The Υ indicator, thus, defines a distance from the limiting random walk-like behavior as a way to assess the dynamical stability properties of an observable. The indicator was applied to atmospheric boundary layer data by Nevo et al.[12] and Kaiser et al.[13] and to atmospheric circulation data by Faranda and Defrance.[14] They successfully demonstrated the indicator's ability to both gauge the stability of a time series and detect tipping points. However, the indicator requires some

additional testing, in particular, concerning its performance for rate-induced tipping, which, thus, far has not been explored. It should be noted that several different early-warning indicators based on ARMA models have been proposed. In fact, in Faranda et al.,[11] the authors propose the sum of the p and q orders of the model as well as the sum of the model coefficients as potential indicators. The sum of the order parameters then gives an estimate for the memory lag of the process, while the sum of the model coefficients gives the persistence of this memory lag.

To further test the indicator, we have chosen the global oceanic three-box model studied by Alkhayuon et al.,[15] which, in turn, is based upon the five-box model of Wood et al.[16] The model represents a simplified Atlantic Meridional Overturning Circulation (AMOC), which transports warm surface water from the tropics to North America and Europe, resulting in a milder climate in these regions than what would otherwise be expected. Since the current is density driven, a large influx of freshwater due to the melting of land ice or increased precipitation in the North Atlantic would be expected to result in a reduction in the AMOC flow strength. The question of whether the AMOC could undergo a sudden transition from a high flow strength state (the "on" state) to a state with weak or no overturning (the "off" state) is still debated. The latest assessment report of the International Panel for Climate Change (IPCC AR6) concludes that the AMOC strength will very likely decline in the future but states with medium confidence that an abrupt collapse will not occur in the next century.[17] Simple box models, such as the one presented in this paper, show bi-stability, while more realistic models, such as the global atmosphere-ocean general circulation models (AOGCMs), are largely mono-stable, implying that they do not exhibit the abrupt transition to an "off"-state so characteristic of the simpler models. However, there is limited evidence that the more complex models may be too stable (Weijer et al.,[18] Hofmann and Rahmsdorf,[19] and Liu et al.[20]), in particular, that they mis-represent the direction of AMOC-induced freshwater transport across the southern boundary of the Atlantic (Liu et al.,[20] Huisman et al.,[21] Liu et al.,[22] and Hawkins et al.[23]). Liu et al.[20] demonstrated that by introducing a flux-correction term into the National Center for Atmospheric Research (NCAR) Community Climate System Model version 3 (CCSM3), they could make the formerly mono-stable system bi-stable.

In addition, it has been suggested that paleoclimate data are consistent with abrupt changes in the surface temperature in the North Atlantic region in the past, as might be expected with a collapse of the AMOC. Boers[24] applied a statistical early-warning indicator on Earth System Model (ESM) outputs and found significant early-warning signals in eight independent AMOC indices. This was interpreted as a sign that the AMOC is not only a bistable system, but one approaching a critical transition.

Previously, the potential collapse of the AMOC has largely been attributed to the crossing of a bifurcation boundary in the bi-stable system. However, more recent analysis, see, in particular, Lohman and Ditlevsen,[25] demonstrate the possibility of tipping before the bifurcation boundary is reached through the mechanism of rate-induced tipping. In addition, Lohman and Ditlevsen,[25] demonstrate that due to the chaotic nature of complex systems, a well-defined critical rate, i.e., the rate of parameter change at which the system tips, cannot be obtained, which, in turn, severely limits our ability

to predict the long-term behavior of the system. They conclude that due to this added level of uncertainty, it is possible that the safe operating space with regard to future emissions of CO_2 might be smaller than previously thought. This suggests that proper evaluation of the probability of rate-induced tipping in the different tipping elements of the Earth System is of utmost importance in assessing the likelihood of dramatic future changes.

Regardless of whether the AMOC in actuality is bi-stable or mono-stable, the reduced five-box model of Alkhayuon et al.[15] is the perfect test case for the Υ indicator as it exhibits both bifurcation-induced and rate-induced tipping, provided a time-dependent hosing function is applied. The hosing function represents the influx of fresh water into the ocean due to increased precipitation and melting of land and sea ice in the North Atlantic region. Alkhayuon et al.[15] provide an extensive analysis of the tipping mechanisms present in the model. Armed with such a well studied theoretical model, we will be able to systematically study the indicator's ability to not only detect bifurcation-induced and noise-induced, but also rate-induced tipping. We will additionally assess the indicator's ability to deal with colored noise, something that is known to cause issues for other early-warning indicators, such as the increase in variance and auto-correlation.[24]

In reality, the ocean system has many more degrees of freedom than those included in the box models, and ultimately, a mixture of different processes is likely to trigger tipping, if occurring. The Coupled Model Intercomparison Project (CMIP6), with the Community Earth System Model (CESM2),[26] provides an alternative AMOC model with many more degrees of freedom. Two scenarios where the atmospheric CO_2 concentration is abruptly increased will be considered, providing monthly outputs of geographical density differences on which the Υ indicator will be applied. In these model scenarios, the abrupt change in CO_2 is followed by a response of the Earth system, and after two to three decades, freshwater eventually circulates in the sub-polar gyre.[27] This response, hence, offers similarities with the hosing experiments done in the box models. While the two scenarios are insufficient to assess the potential bistability of the AMOC, the Υ indicator will be used to assess the dynamical stability of the AMOC during its weakening phase.

II. THE Υ-INDICATOR FOR EARLY-WARNING SIGNALS

In what follows, we will briefly outline the method used to determine the stability of the time series data. Further details can be found in Faranda et al.,[10] Faranda and Defrance,[14] Nevo et al.,[12] and Kaiser et al.[13]

The method relies on an accurate representation of a complex dynamical system close to a metastable state by a random walk-like behavior with a tendency to be attracted to the metastable state. Changes in the system's stability are then characterized as statistically significant deviations from that local behavior, indicating that the system currently does not reside close to a metastable state. Indeed, the local dynamics of a continuous-time random dynamical system (i.e., a stochastic differential equation) near a metastable state come close to the dynamics of a stochastic spring (i.e., an Ornstein–Uhlenbeck process), whose discrete-time observations are well approximated by an ARMA (1,0) process. Here, ARMA denotes the space of autoregressive moving-average models,

with the numbers in parentheses denoting the order of the model. A time series $x(t)$, $t \in \mathbf{Z}$, is an ARMA(p,q) process if it is stationary and can be written as

$$x(t) = \nu + \sum_{i=1}^{p} \phi_i x_{t-i} + \sum_{j=1}^{q} \theta_j w_{t-j} + w_t, \tag{1}$$

with constant ν, coefficients ϕ_i, θ_j, and $\{w_t\}$ being white noise with positive variance σ^2 (see Brockwell and Davis[28] for an introductory text). In addition, constraints are imposed on the coefficients ϕ_i and θ_j to ensure that the process in (1) is stationary and satisfies the invertibility condition. Intuitively, the variables p and q say something about the memory lag of the process, while the prefactors ϕ_i and θ_j relate to the persistence of the said memory lag. One expects that the higher the values for q and p, the longer the system, once perturbed from its equilibrium state, would need to return to equilibrium. It is this intuitive notion that the statistical indicator denoted Υ takes advantage of. Indeed, when approaching a critical transition, the response of the system to perturbations can become increasingly long (referred to as a critical slow down), and this translates into diverging memory properties of the statistical signal. Hence, an ARMA(p,q) model will require higher orders to incorporate the memory effects. By fitting the model (1) repeatedly to a time series data set for varying values of p and q, one can, through application of an appropriate information criterion, obtain the values of p and q that best represent the time series data. For this purpose, we choose the Bayesian information criterion, BIC,

$$\mathrm{BIC} = -2 \ln L(\hat{\beta}) + \ln(\tau)(p + q + 1), \tag{2}$$

where $\hat{\beta}$ denotes the maximum likelihood estimator of $\beta = (\nu, \phi_1, \ldots, \phi_p, \theta_1, \ldots, \theta_q)$, which is obtained by maximizing the likelihood function L associated with the ARMA(p,q) model (1) for a given time series; see Brockwell and Davis[28] for details. The best-fitting ARMA(p,q) model is then determined as the one that minimizes the BIC. The second term in Eq. (2) punishes complex models with high p and q values and is the reason why we prefer to use the BIC over other criteria, such as perhaps the more familiar Akaike information criterion. Here, τ denotes the number of discrete points in the time series to which the ARMA model is fitted. We refer to τ as the *window length*.

Finally, the stability indicator is defined as

$$\Upsilon(p, q; \tau) = 1 - \exp\left(\frac{-\left|\mathrm{BIC}(\bar{p}, \bar{q}) - \mathrm{BIC}(p, q)\right|}{\tau}\right), \tag{3}$$

where $\bar{p}$ and $\bar{q}$ indicate the order of what we refer to as the theorized *base model*. This is the ARMA(p,q) model, characterized by a specific value of $q = \bar{q}$ and $p = \bar{p}$, to which the chosen best fit is compared. The Υ-indicator takes on values between 0 and 1, where lower values imply a higher degree of stability. The intuition behind using the difference in BIC values between the chosen "best" model and a base model is that this quantity assesses just how much better the model with the lower BIC value approximates the fitted data compared to the other. The significance threshold for deviations in the BIC values between an ARMA(p,q) and the base model, simply denoted as $|\Delta \mathrm{BIC}|$, is $|\Delta \mathrm{BIC}| > 2$. The differences in BIC values can be directly related to the Bayes factor; see Preacher and Merkle,[29]

which is another way of quantifying the likelihood of one model over another.

For the data sets analyzed by Faranda *et al.*,[10] it was determined that the appropriate base model is the ARMA(1,0) model, i.e., $\bar{p} = 1$ and $\bar{q} = 0$, which can be viewed as a time discretized Langevin process. In the later work by Nevo *et al.*[12] and Kaiser *et al.*,[13] the authors continued to rely on ARMA(1,0) as the base model. While Faranda *et al.*[10] used a statistical argument to justify the choice of the base model, Nevo *et al.*[12] and Kaiser *et al.*[13] argued, as already noted above, that the dynamics near a stable state can be approximated as that of a stochastic spring, further strengthening the case for ARMA(1,0) as the general choice of the base model. However, due to the additional well-posedness constraints on the autoregressive and moving-average coefficients ϕ_i and θ_j in (1), depending on the treatment of constraints by the fitting routine, one can have cases where the BIC value of the ARMA(1,0) process is smaller than the corresponding value for the chosen ARMA(p,q) model. In these cases, the ARMA(1,0) process is rejected as the best fit, despite having the lowest BIC value, due to violating the stationarity or invertibility conditions required for a numerically well behaved fit. Thus, in this scenario, it becomes unclear how to determine the "distance" between the states. To overcome this issue, we have chosen to modify the Υ indicator to allow for a second base state, namely, the ARMA(0,0) model. This model is just white noise, possibly with a drift, and is guaranteed to satisfy all the auxiliary conditions for the obvious reasons that there are no coefficients available to violate them. We consider ARMA(0,0) as a special case of ARMA(1,0) in which $\phi_1 = 0$. The use of the ARMA(1,0) process as a base model was partly justified by the image of a particle trapped in a potential well, where a restoring force keeps the particle oscillating around the equilibrium. The justification for including ARMA(0,0) as a potential base model follows a similar argument except that in this case, the noise amplitude is too low compared to the width of the potential well to feel the restoring force. To use both base models, we first introduce

$$\Delta \text{BIC}_0(p,q) := \text{BIC}(0,0) - \text{BIC}(p,q) \qquad (4)$$

and

$$\Delta \text{BIC}_1(p,q) := \text{BIC}(1,0) - \text{BIC}(p,q). \qquad (5)$$

With this, the modified Υ-indicator for the extended base model class can be written as

$$\Upsilon(p,q;\tau) = 1 - \exp\left(\frac{-\min\left\{|\Delta \text{BIC}_0(p,q)|, |\Delta \text{BIC}_1(p,q)|\right\}}{\tau}\right). \qquad (6)$$

In addition, it must be specified that in the cases where the constrained fitting failed for the ARMA(1,0) model so that $\Delta \text{BIC}_1(p,q)$ may be negative, $\Delta \text{BIC}_0(p,q)$ is automatically chosen in practice. For obvious reasons, there cannot be a case where $\Delta \text{BIC}_0(p,q)$ is itself negative.

Furthermore, following Faranda *et al.*,[11] we define the *order*, $\mathscr{O}$, and *persistence*, $\mathscr{R}$, of an ARMA(p,q) process as

$$\mathscr{O} = p + q, \qquad (7)$$

$$\mathscr{R} = \sum_{i=1}^{p} |\phi_i| + \sum_{i=1}^{q} |\theta_j|, \qquad (8)$$

where ϕ_i and θ_j denote the autoregressive and moving-average coefficients, respectively. While the order relates to the memory lag of the process, the persistence relates to the *persistence* of the said memory lag, hence the name. When approaching a tipping point, one would expect one out of two things to happen: either both the persistence and the order increase significantly, due to the increased memory of the process, or the order remains constant, and the persistence approaches the value of the order $\mathscr{O}$, indicating a loss of stationarity. According to Faranda *et al.*,[11] the latter alternative corresponds to a case in which the potential landscape of the system does not change considerably when approaching the transition.

This observation strengthens the case for the modified Υ indicator in contrast to excluding windows of the time series where $\Delta \text{BIC}_1(p,q)$ is negative, as these periods are indicative of an instability resulting from the loss of stationarity of the ARMA(1,0) process.

To apply the method to a time series data set, one first has to ensure stationarity of the data. This can be done in two ways depending on the nature of the time series. In some cases, it is sufficient to split the time series into small enough intervals so that within each interval, the time series is approximately stationary. To check for stationarity, one runs Kwiatkowski–Phillips–Schmidt–Shin (KPSS) tests on the intervals. This way, one also obtains an upper bound on the length of the intervals; see Kaiser *et al.*[13] The other option is to not assume stationarity from the outset and instead allow for application of a differencing routine to the separate intervals, achieving stationarity that way. In that case, a KPSS test is run on each interval, and if the interval is found to not be stationary, differencing is applied. This process is then repeated until stationarity is achieved. The KPSS test is to be preferred over the unit root test due to the danger of over-differencing (Hyndman and Khandakar[30]). As we wish to study rate-induced tipping phenomena, which yield highly nonstationary time series even for very small interval lengths, the latter method is to be preferred. By this choice, we go from an ARMA to an ARIMA model, in which the I stands for "integrated" in reference to the differencing routine used to ensure the stationarity of the time series.

Provided one can select sufficiently long time series intervals where the process is approximately stationary, one can fit ARMA(p,q) models to available observations during these intervals, and through the Υ indicator, one can obtain an estimate for how close any given interval is to an equilibrium state. To determine the best fit, we use the auto.arima function found in the FORE-CAST R package, setting BIC as the information criterion used for model selection. Since we will not assume stationarity of the time series, auto.arima first determines the correct differencing order before continuing with the fitting procedure; the details of the said procedure can be found in Hyndman and Khandakar.[30]

It is clear that the method is strongly dependent upon the size of the intervals, which we will refer to as the window length, τ. This is not only due to the inclusion of the $1/\tau$ factor in the exponential, but also due to the inherent τ-dependence of BIC(p,q) and BIC(1,0). In fact, the rationale for including the $1/\tau$ factor in the definition of Υ is to attempt to remove or reduce this dependence. From equation (2), one might conclude that the correct scaling would be $1/\ln(\tau)$, as opposed to $1/\tau$. However, we do not only want to remove the dependence on τ, but also include the significance threshold for
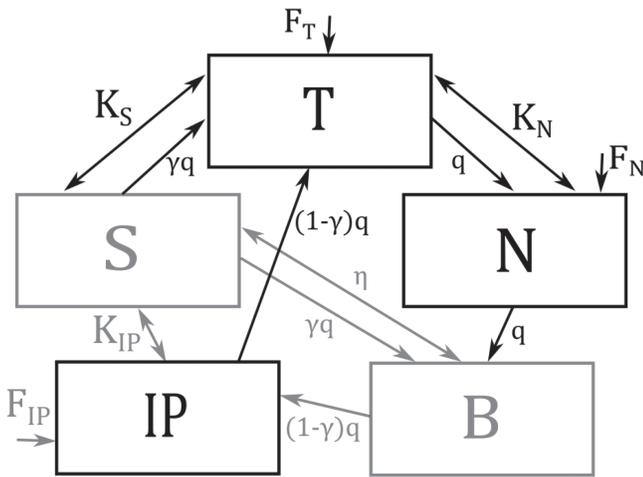
FIG. 1. Sketch of the five-box model for the Atlantic Meridional Overturning Circulation (AMOC). Here, light gray coloring is used to denote the two boxes whose salinities do not change as well as all the arrows, indicating terms that do not appear in the equations describing the dynamics of the three-box model. Adapted from Alkhayuon *et al.*, Proc. R. Soc. A **475**, 20190051 (2019). Copyright 2019 The Royal Society.[15]

ΔBIC such that the Υ value of any point where ΔBIC is below 2 is suppressed relative to other points.

III. APPLICATION TO THE GLOBAL OCEANIC THREE-BOX MODEL

To determine the validity of the Υ-indicator as a measure of stability as well as its ability to detect different types of tipping points, we start by applying the method to the global oceanic three-box model discussed by Alkhayuon *et al.*[15] The three-box model of Alkhayuon *et al.*[15] is a simplification of the five-box model of Wood *et al.*[16] in which the salinity of the Southern Ocean (S) and the Bottom waters (B) is assumed to be approximately constant. The model, thus, consists of five separate boxes, of which only three boxes, namely, the North Atlantic (N), the Tropical Atlantic (T), and the Indo-Pacific (IP) boxes have varying salinities S. A schematic illustration of the model is shown in Fig. 1. See Alkhayuon *et al.*[15] or Wood *et al.*[16] for a detailed exposition of the box model. We note that the parameters of the box model are tuned using the full complexity FAMOUS AOGCM model, with varying levels of CO_2. The parameters used in this paper are for the case $2 \times CO_2$ as compared to pre-industrial times.

We denote salinity by S_i, the volume by V_i, and the fluxes by F_i, where $i \in \{N, T, S, IP, B\}$ denotes the respective boxes.

Let Γ denote the AMOC flow defined by

$$\Gamma = \lambda \left[\alpha(T_S - T_0) + \frac{\beta}{100}(S_N - S_S) \right]. \quad (9)$$

The model approximates a buoyancy-driven flow, with a transport proportional to the density difference between the boxes, assuming a linearized equation of state. The evolution equations for the

TABLE I. Numerical values for volume, salinity and fluxes as used in the 3-box model. Adapted from Alkhayuon *et al.*, Proc. R. Soc. A **475**, 20190051 (2019). Copyright 2019 The Royal Society.[15]

	Volume (m³)	Salinity	Flux (Sv)
North Atlantic	$V_N = 0.3683 \times 10^7$	$S_N = 0.034\,912$	$F_N = 0.486$
Tropical Atlantic	$V_T = 0.5418 \times 10^7$	$S_T = 0.035\,435$	$F_T = -0.997$
Southern Ocean	$V_S = 0.6097 \times 10^7$	$S_S = 0.034\,427$	$F_S = 1.265$
Indo-Pacific	$V_{IP} = 1.4860 \times 10^7$	$S_{IP} = 0.034\,668$	$F_{IP} = -0.754$
Bottom Ocean	$V_B = 9.9250 \times 10^7$	$S_B = 0.034\,538$	

salinities S_N and S_T are

$$\frac{V_N}{Y}\frac{dS_N}{dt} = \Gamma(S_T - S_N) + K_N(S_T - S_N) - 100F_N S_0, \quad (10)$$

$$\frac{V_T}{Y}\frac{dS_T}{dt} = \Gamma[\gamma S_S + (1-\gamma)S_{IP} - S_T] + K_S(S_S - S_T)$$
$$+ K_N(S_N - S_T) - 100F_T S_0 \quad (11)$$

for $\Gamma \geq 0$ and

$$\frac{V_N}{Y}\frac{dS_N}{dt} = |\Gamma|(S_B - S_N) + K_N(S_T - S_N) - 100F_N S_0, \quad (12)$$

$$\frac{V_T}{Y}\frac{dS_T}{dt} = |\Gamma|(S_N - S_T) + K_S(S_S - S_T) + K_N(S_N - S_T) - 100F_T S_0 \quad (13)$$

for $\Gamma < 0$, where S_B and S_S are regarded as fixed parameters and $Y = 3.15 \times 10^7$, which converts the time unit from seconds to years. S_0 is a reference salinity, and K_i are coefficients associated with the gyre strengths. We note that all the salinity values are given as perturbations from a background state; see Appendix A of Alkhayuon *et al.*[15] for details on the transformation. Since the total salinity is assumed to be conserved, the salinity of the Indo-Pacific (IP) box, S_{IP}, can be computed from S_N and S_T.

The values of the assorted parameters can be found in Tables I and II.

TABLE II. Numerical values for the parameters used in the 3-box model. Adapted from Alkhayuon *et al.*, Proc. R. Soc. A **475**, 20190051 (2019). Copyright 2019 The Royal Society.[15]

Name	Default value	Units	Name	Default value	Units
α	0.12	kg/(m³ °C)	K_N	1.762	Sv
β	790.0	kg/m³	K_S	1.872	Sv
S_0	0.035		λ	1.62×10^7	m⁶/(kg s)
T_S	7.919	°C	γ	0.36	
T_0	3.870	°C			

The fluxes, F_N and F_T, are linear functions of the hosing function $H(t)$, which simulates the influx of fresh water. In the case of $2 \times CO_2$, the fluxes are (see Wood et al.[16])

$$F_N = 0.486 \times 10^6 + H(t)\, 0.1311 \times 10^6, \tag{14}$$

$$F_T = -0.997 \times 10^6 + H(t)\, 0.6961 \times 10^6, \tag{15}$$

where all fluxes are given in units of Sverdrup (Sv).

The values for the case of $1 \times CO_2$ can be found in Table 5 of Alkhayuon et al.[15]

Figure 3 shows the bifurcation diagram for S_N; for S_T, we refer to Alkhayuon et al.[15] The bifurcation diagram for the flow strength Γ is qualitatively similar since all other parameters in Eq. (9) are kept constant. The diagram clearly shows that this is a bi-stable system with two stable equilibrium branches connected by an unstable branch. The upper equilibrium branch loses stability, not at the saddle-node bifurcation, but rather due to a Hopf bifurcation, indicated by a red diamond in the diagram. Thus, part of the upper equilibrium branch, denoted in black, is, in fact, unstable.

To simulate the influx of fresh water, we apply a time-dependent, piece-wise linear hosing function, $H(t)$ (see Fig. 2), to Eqs. (10)–(13). Here,

$$H(t) = \begin{cases} H_0 & t < 0, \\ H_0 + \alpha(t), & t \in [0, T_{rise}], \\ H_{pert}, & t - T_{rise} \in [0, T_{pert}], \\ H_{pert} - \beta(t), & t - T_{rise} - T_{pert} \in [0, T_{fall}], \\ H_0, & t \geq T_{rise} + T_{pert} + T_{fall}, \end{cases} \tag{16}$$

where $\alpha(t)$ and $\beta(t)$ are linear functions ensuring continuity of $H(t)$. If we define the rise and fall rates as

$$r_{rise} = \frac{|H_{pert} - H_0|}{T_{rise}} \quad \text{and} \quad r_{fall} = \frac{|H_{pert} - H_0|}{T_{fall}}, \tag{17}$$

then

$$\alpha(t) = r_{rise} t \quad \text{and} \quad \beta(t) = r_{fall}(t - T_{rise} - T_{pert}). \tag{18}$$

As demonstrated by Alkhayuon et al.,[15] whether the system undergoes a transition from one stable state to the other is dependent not only on the value of H_{pert}, but on the rise and fall rates, r_{rise} and r_{fall}, as well as the perturbation time T_{pert}. In particular, they demonstrate that even when H_{pert} is above the bifurcation value that destabilizes the upper equilibrium branch, the system may still return to this equilibrium, provided T_{fall} is short enough; a process that they termed *avoided B-tipping*. In addition, they showed that if T_{pert} is too short, the system will not tip, but return to the initial equilibrium branch.

In what follows, we will apply the Υ indicator as described in Sec. II to time series data generated by the three-box model. We will separately study time series undergoing rate-, noise-, and bifurcation-induced tipping, while attempting to assess the indicator's ability to gauge the stability of the time series as it approaches the tipping point. Before proceeding, we should clarify one point regarding noise-induced tipping and what is meant by an early-warning indicator in this context. Noise-induced tipping is inherently unpredictable, and hence, one might conclude that any attempt at predicting such transitions is doomed to fail based on a single
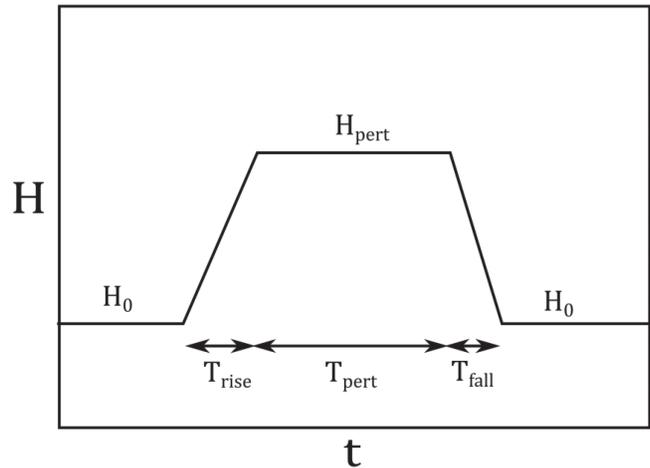

FIG. 2. Schematic illustration of the piece-wise linear hosing function used to simulate the influx of fresh water. Adapted from Alkhayuon et al., Proc. R. Soc. A **475**, 20190051 (2019). Copyright 2019 The Royal Society.[15]

time series. In contrast, assuming the underlying model is known, one could use ensembles of realizations to estimate the likelihood of noise-induced transitions. Examples of these statistical approaches are discussed in Thompson and Sieber.[31]

Although one cannot expect to develop an *early* warning indicator for these types of transitions, one should at the very least be able to tell, from time series data, once such a transition has occurred, i.e., when the unstable equilibrium branch has been crossed and the system is approaching a different equilibrium. The objective should then be to develop an indicator that is able to identify this induced instability as soon as possible after the transition.

Finally, we note that, while it is possible to extend ARMA fitting to multivalued time series data, we have chosen to not go down that
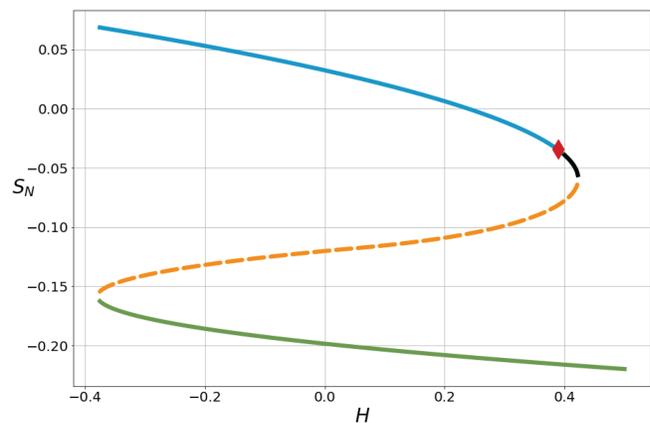

FIG. 3. Bifurcation diagram for S_N for the three-box model of the AMOC. The dashed line denotes the unstable equilibrium branch. The red diamond denotes the location of the Hopf-bifurcation.
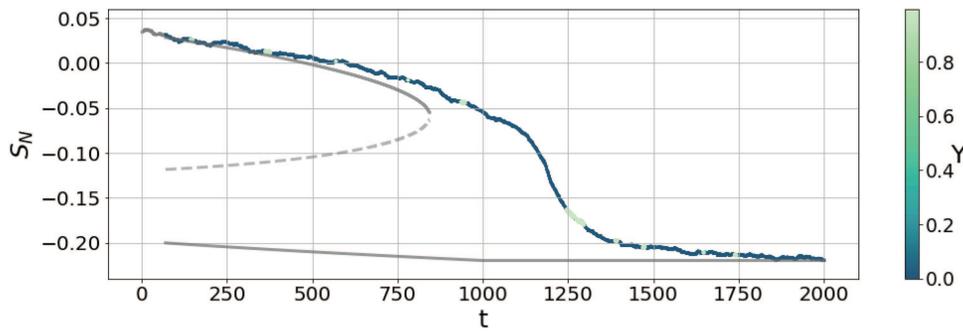
FIG. 4. Bifurcation-induced tipping, color coded according to the value of Υ with window length, $\tau = 350$. The gray lines denote the equilibrium branches, with the dashed line corresponding to the unstable branch. We clearly see several brightly colored points corresponding to high values of Υ, which should be indicative of a high degree of instability and an approaching tipping point.

route and instead only apply the indicator to a single time series for the salinity values from the North Atlantic basin, S_N. The reason for choosing S_N over S_T is that within the three-box model, the equilibrium branches of S_N are that much further apart, making the transitions easier to see. Such a simplification might at first glance seem rather contrived; however, we argue that, as the goal of any indicator is to be used on real-world time series data in which the connection to other time series is largely unknown, it is reasonable to only concentrate on one time series despite the underlying system being multidimensional.

A. Bifurcation-induced tipping

To induce B-tipping in the three-box model, we gradually change $H(t)$ according to equation (16), with $H_0 = 0$, $H_{pert} = 0.5$, $T_{rise} = 1000$. This corresponds to an increase in the freshwater fluxes F_T and F_N, corresponding to the flux into the tropical and North Atlantic boxes, by approximately 34% and 13%, respectively. This, in turn, corresponds to roughly a 0.1–0.2 Sv increase, in line with freshwater "hosing" experiments of the North Atlantic, e.g., Ref. 32. We let T_{pert} go to infinity such that $H(t)$ never returns to its initial value. As $H(t)$ changes, S_N follows the upper equilibrium branch as sketched in Fig. 3, until it reaches the Hopf bifurcation (around $H = 0.4$), at which point the upper equilibrium branch becomes

unstable, and S_N starts approaching the lower equilibrium branch. We choose a window length of 350 points corresponding to about 70 years.

Figure 4 shows the time series of S_N color coded according to the value of Υ, with brighter colors corresponding to higher values of Υ and, hence, a greater degree of instability. Figure 5 shows Υ as a function of time, with clear peaks corresponding to brightly colored points in Fig. 4.

It should be noted that low amplitude white noise is also applied to facilitate ARIMA model fitting. The noise intensity is kept small enough to avoid noise-induced tipping.

Figures 4 and 5 clearly indicate that there are several points on the time series as it approaches the transition, which are deemed to have a high degree of instability. We further note that, although the result is not shown here, the high Υ values in Figs. 4 and 5 correspond to intervals for which $\Delta \mathrm{BIC}_1(p, q)$ is negative, indicating that, as discussed previously, the ARMA(1,0) model would, when only considering BIC values, be the better fit, but it violates the auxiliary conditions, indicating a loss of stationarity. Hence, at these points, ARMA(1,0) is excluded as a possible model, implying that ARMA(0,0) is the chosen base model.

In addition, we look at the order of the best-fit ARMA model, namely, the q and p values, as well as the persistence, to gain further insight into the stability properties of the time series. Figure 6
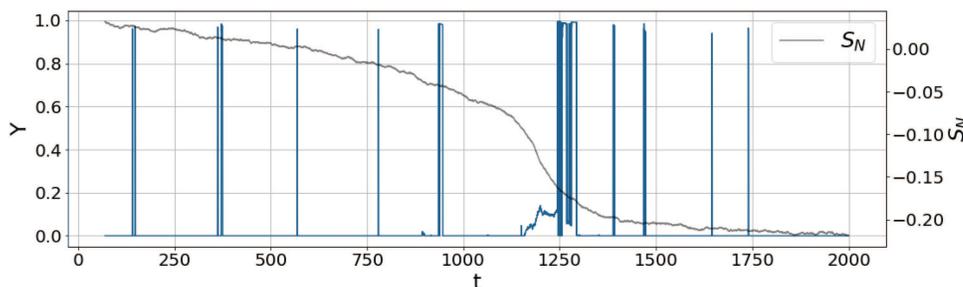

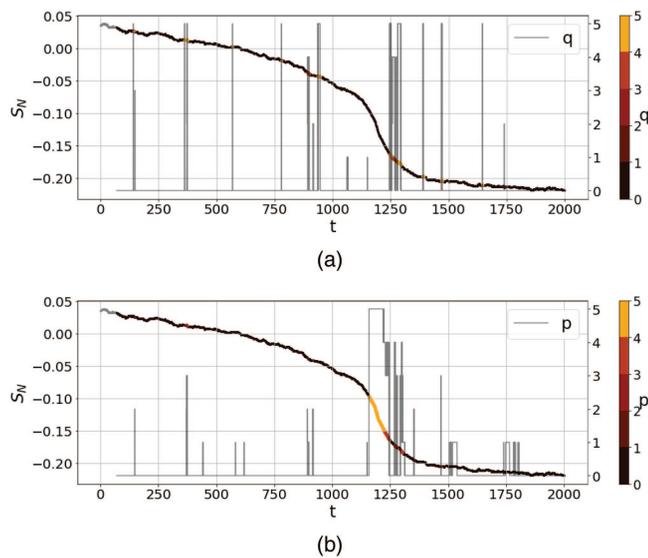**FIG. 5.** Υ as a function of time for a time series of S_N undergoing B-tipping.

FIG. 6. Bifurcation-induced tipping of $S_N(t)$, color coded according to the value of the best-fit ARMA model orders (a) q and (b) p (scatterplot). The line plots additionally show the same values for q and p as functions of time in (a) and (b), respectively.

shows the time series of S_N color coded according to the values of q and p. When comparing with Fig. 4, this seems to indicate that the high values of Υ appearing before the transition are primarily associated with an increase in the q-values. This is not unexpected, as it is primarily the change in the properties of the noise, which is expected to give an indication of an approaching transition. Figure 7 shows the persistence plotted as a function of time t. We see a clear increase in the persistence directly preceding the tipping point around $t = 1000$.

We make a final comment regarding Fig. 6 and its relation to our choice of ARMA(1,0) and ARMA(0,0) as base models. In Faranda et al.,[10] this choice was guided by the fact that for the time series under consideration, the order, i.e., $p + q$, of the intervals was clustered around 1, and as the authors explicitly excluded pure moving-average processes, they concluded that ARMA(1,0) was the appropriate base model. However, from Fig. 6, we see that for the

time series currently under consideration, the order is clustered around 0. This observation further strengthens the case for using ARMA(0,0) as an additional base model. We hypothesize that the dominance of ARMA(0,0) is related to the low degree of noise in the system, which makes the restoring force that returns the system to equilibrium less prominent, hence obscuring tendency of the random walk to be attracted to a metastable state.

B. Noise-induced tipping

To induce N-tipping, we fix the hosing parameter H and apply additive white noise to all the equations equally. The noise term is added equally to (10)–(13), with the same noise amplitude in all cases. We look at transitions from the upper branch to the lower branch and vice versa. In either case, it is convenient to choose a value for H that is close to the bifurcation point, as the probability of transitioning is much higher in these regions, and hence, one does not need high amplitude noise to induce transitions between the branches.

Figures 8 and 9 show two time series undergoing noise-induced tipping, one going from the lower to the upper branch, while the other going the other way around. In the first case, $H = -0.25$, while in the second, $H = 0.24$. The amplitude of the additive white noise is the same in both cases. For the window length τ, we have chosen a length of 350 and 200 points, corresponding to about 70 and 41 years, respectively. The window length is chosen so that it is at most half as long as the transition time, which is taken to be the time for the system to arrive at the other equilibrium once it has crossed the unstable branch. Of course, when dealing with simulation data, such as these, we have the advantage of knowing where the stable and unstable branches are, which is an advantage that anyone dealing with real-world data does not have. In principle, one could use the clustering methods proposed by Kaiser et al.[13] to approximate the window length, although this method also requires that one knows how many clusters, i.e., equilibrium states, one should look for. The clustering method works particularly well for noise-induced transitions, as one can repeatedly induce transitions back and forth to gain an ensemble of transitions, yielding a higher degree of accuracy.

In previous works, the choice of τ has largely been guided by a desire to ensure the stationarity of the time series intervals. However, as we are not requiring the individual time series segments to be stationary a priori, we are permitted to use much longer time
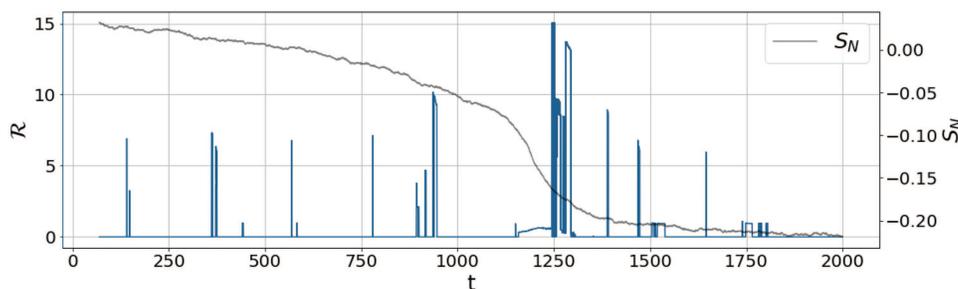

FIG. 7. Plot of the persistence $\mathcal{R}$ [Eq. (8)] as a function of time for a time series of S_N undergoing B-tipping.
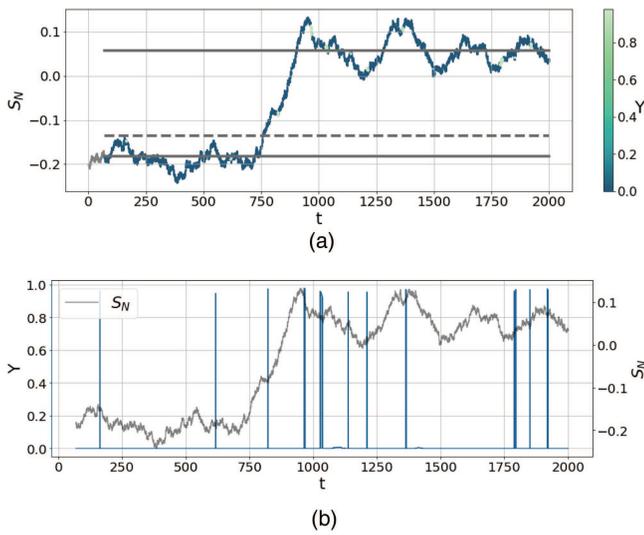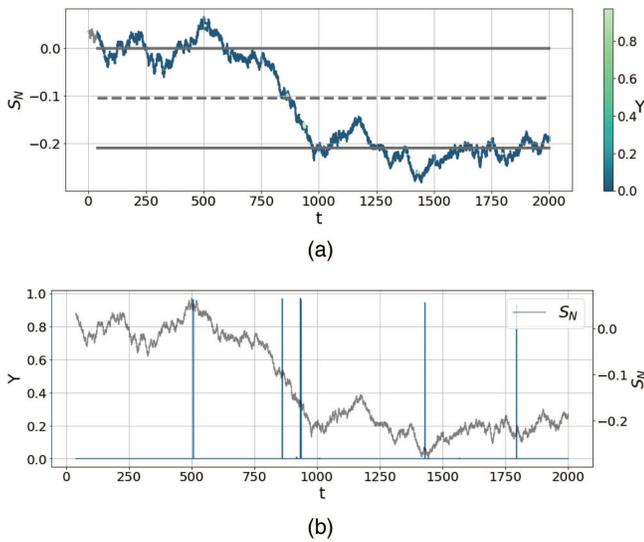
FIG. 8. (a) Noise-induced tipping, color coded according to the value of Υ. The gray lines denote the equilibria, with the dashed line denoting the unstable equilibrium branch. Transition from the lower to upper equilibrium branch for $H = -0.25$, $\tau = 350$. (b) Plot of Υ as a function of time. Note how the peaks correspond to the brightly colored points in (a).
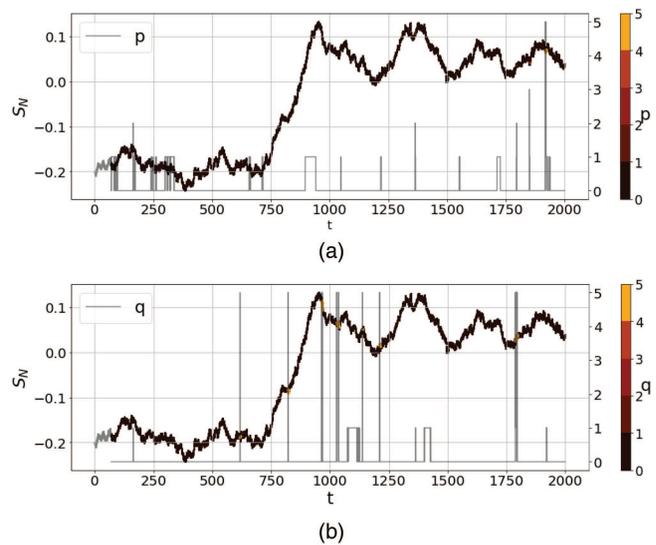

FIG. 10. Noise-induced tipping of $S_N(t)$ for $H = -0.25$, $\tau = 350$, color coded according to the value of (a) p and (b) q. For clarity, we have also plotted p and q as functions of time in (a) and (b), respectively.

series intervals. In the world of ARIMA fitting, a time series of length above 200 points would generally be considered a very long series; however, we should keep in mind that the sampling frequency of our simulated data is quite high; in fact, there are 5 points per time

FIG. 9. (a) Noise-induced tipping, color coded according to the value of Υ. The gray lines denote the equilibria, with the dashed line denoting the unstable equilibrium branch. Transition from the upper to lower equilibrium branch for $H = 0.24$, $\tau = 200$. (b) Plot of Υ as a function of time. Note how the peaks correspond to the brightly colored points in (a).

unit (i.e., year), yielding a total of 10 000 points for the 2000 years of simulations. An interval consisting of 200 points corresponds to around 40 years, which is not an unreasonably long time interval for the dynamics of the AMOC. When fitting an ARIMA model to a time series, one wishes to avoid too long time series to avoid, including events from the past that no longer have any relevance for the future. This, and not the inherent inaccuracy of the fit itself, is the primary reason for limiting the length of a time series.

Returning to Figs. 8 and 9, we note that there are a few brightly colored points indicating a high degree of instability. There are, for example, in both cases, several points in the middle of the gap between the two stable branches, indicated by solid gray lines in the figure. This is consistent with the results of Kaiser *et al.*[13] In addition, for the transition from the lower to upper branch, Fig. 8, there are several brightly colored points just after the system has reached the upper equilibrium branch. Although it is not so clear in the figure due to the presence of noise, any time S_N returns to the upper equilibrium branch it initially overshoots and then oscillates around the equilibrium value with continuously decreasing amplitude (see Fig. 13 for a clearer example of this behavior). This is probably due to the presence of an unstable limit cycle and the aforementioned sub-critical Hopf bifurcation. Hence, we see it as an encouraging sign that the indicator seems to be able to identify these points as well. We further note that, although the result is not shown, the high Υ value points in Figs. 8 and 9 correspond to points where $\Delta_1 \text{BIC}(p, q)$ is negative, as was the case for the B-tipping example in Sec. III A.

Looking at the p and q values in Figs. 10 and 11, it is clear that high values of Υ correspond to high values of q, while the connection between p and Υ remains uncertain. However, we note
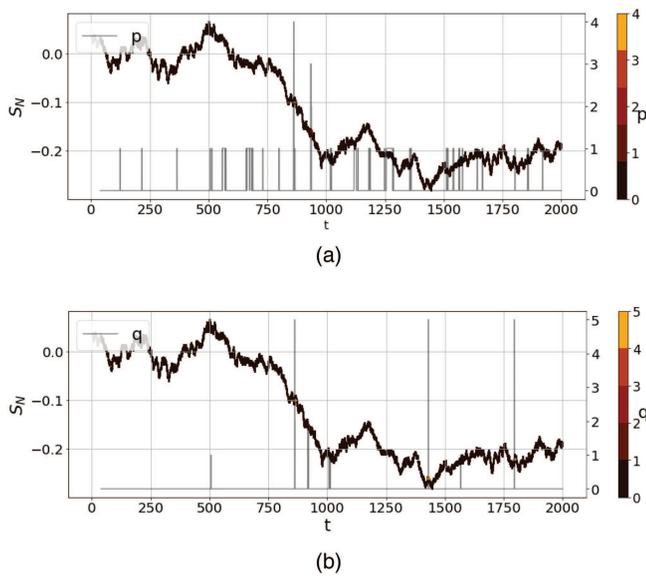
(a)

(b)

FIG. 11. Noise-induced tipping of $S_N(t)$ for $H = 0.24$, $\tau = 200$, color coded according to the value of (a) p and (b) q. For clarity, we have also plotted p and q as functions of time in (a) and (b), respectively.

that the high Υ values appearing around the transition correspond to high values of both p and q and consequently also of persistence (result not shown).

C. Rate-induced tipping

To induce R-tipping, we fix H_{pert} below the bifurcation value, ensuring that both equilibria still exist and are stable and vary T_{fall}. We set $T_{rise} = 100$ and $T_{pert} = 400$, while $H_{pert} = 0.37$. This corresponds to an increase in the freshwater fluxes F_T and F_N, corresponding to the flux into the tropical and North Atlantic boxes, by approximately 25% and 10%, respectively. Next, we observe that for $T_{fall} = 280$, the system returns to the upper equilibrium branch, while for $T_{fall} = 320$, the system transitions to the lower branch. The transition happens even though the bifurcation boundary has not been crossed. Again, we note that some additive white noise has been applied to allow for ARIMA fitting.
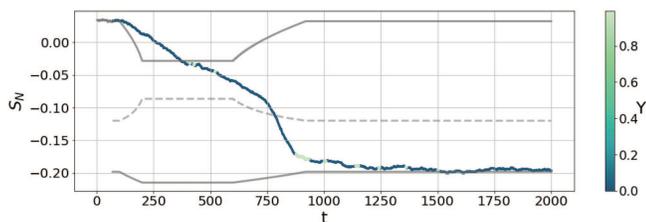

FIG. 12. Rate-induced tipping of S_N, color coded according to the value of Υ. The moving equilibria are plotted in gray, with the dashed line denoting the unstable branch. Compare this figure to Fig. 14(a), which shows the same time series, but color coded according to the value of q.
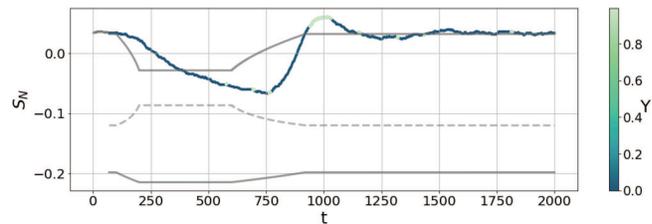

FIG. 13. S_N as a function of time, color coded according to the value of Υ for $T_{fall} = 280$. With these parameter values, the system does not tip but returns to the upper equilibrium branch after some time. Note that the system initially overshoots the stable branch upon return. This is probably due to the presence of the unstable limit cycle. The equilibrium branches are plotted in gray, with the dashed line denoting the unstable branch.

Figure 12 shows a time series undergoing rate-induced tipping, with the color coding corresponding to the values of Υ. Again, we have chosen $\tau = 350$ points, corresponding to 70 years. We see several brightly colored points, indicating a high degree of instability, before the system transitions. These points occur initially as the system approaches the unstable branch (between approximately $t = 350$ and $t = 500$). These points do not appear for the time series that does not tip, Fig. 13, despite the fact that within this time interval, the two time series are virtually identical and could, therefore, be an indication of an approaching tipping point. However, again looking at Fig. 13, we see some brightly colored points, corresponding to large Υ, in the interval $t = 600$ to $t = 750$, and it is unclear what approaching instability these points would be indicative of and, thus, might be regarded as false signals.

Looking at Fig. 14, it becomes clear that the high values of Υ found in Fig. 12 correspond to high values of q, while a comparison with Fig. 16 gives the same indication for the persistence. In other words, high values of Υ primarily correspond to high values of persistence and q.

From Fig. 13, we can also see how the indicator correctly identifies the unstable limit cycle, which we have argued causes the overshoot when returning to the upper equilibrium branch. Figure 15 shows the same time series as in Fig. 13, color coded according to the values of q and p. While high values of q seem to be associated with increased instability, the high values of p primarily occur as the system returns to the equilibrium. We would, therefore, suggest that high values of the autoregressive order, p, should be interpreted as an indication that the system is following a moving equilibrium branch. Comparing Figs. 16 and 14(a), it becomes clear that the points with a high q value around $t = 1000$ correspond to particularly high values of persistence, even when compared to other points of similar order. We also note, as in the previous two tipping scenarios, the high Υ values or, equivalently, high p values.

We end this section with a brief comment on the rate-induced tipping example presented in this section. In this example, the system is, as it undergoes rate-induced tipping, approaching a bifurcation boundary. It would be instructive to study a case in which this is not the case to ensure that the detected instability is not merely due to the approaching bifurcation boundary. However, as one would need to look at different model examples than those presented here, this is outside the scope of the current work.
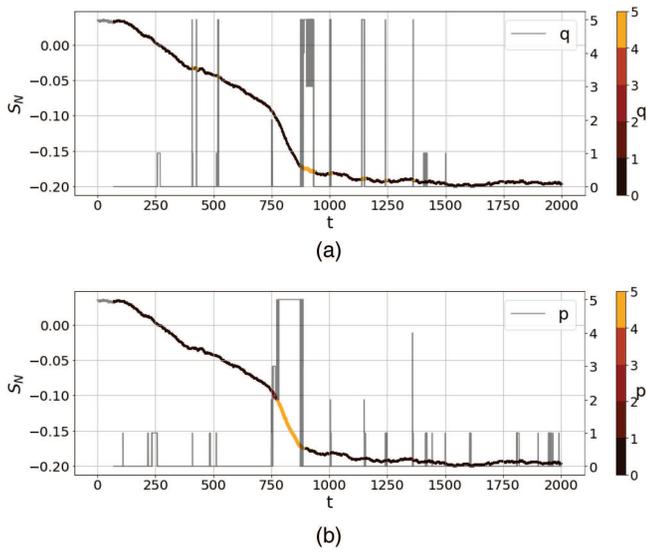
FIG. 14. Rate-induced tipping of $S_N(t)$, color coded according to the value of (a) q and (b) p. The values for q and p are also plotted as functions of time in (a) and (b), respectively.

IV. COMPARISON WITH OTHER EARLY-WARNING INDICATORS

As briefly alluded to in Sec. I, it is well established that bifurcation-induced tipping is generally preceded by an increase in lag 1 autocorrelation and variance (Lenton *et al.*,[33] Dakos *et al.*,[34] and
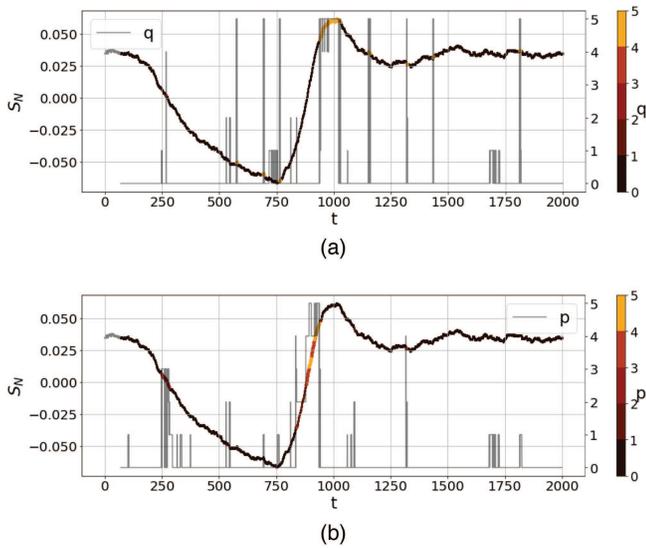

FIG. 15. S_N as a function of time, color coded according to the value of (a) q and (b) p for $T_{fall} = 280$. For these parameter values, the system does not tip but returns to the initial equilibrium after some time t. For clarity, p and q are also plotted as functions of time in (a) and (b), respectively. It is instructive to compare these plots to Fig. 13.

Boers[24]). The intuition behind this is that as the system approaches a bifurcation point, the potential well flattens out, reducing the speed at which the system recovers from a perturbation, so-called critical slowing down, which should manifest as an increase in the variance and autocorrelation of the time series. However, the variance and autocorrelation might also increase for other reasons, in particular, if the properties of the noise change. What happens to the autocorrelation and variance when the system approaches a rate-induced tipping point is, thus, far unclear, although it is conceivable that the "critical slowing down" hypothesis still holds for this type of tipping; see Ritchie and Sieber.[9] Obviously, it does not hold true for time series undergoing purely noise-induced tipping, as there is no change in the potential well. However, the autocorrelation and variance of the time series will dramatically change as the system crosses the unstable equilibrium branch and enters a different potential well.

In what follows, we will compare these classical indicators to the Υ indicator for rate-induced and bifurcation-induced tipping in the AMOC three-box model. It is instructive to just look at the part of the time series prior to the transition, as in general, one wishes to be able to detect early signs of the transition *before* it happens. For the time series undergoing bifurcation-induced tipping (Fig. 4), we chose a segment consisting of the points between approximately $t = 200$ and $t = 1100$. For the time series undergoing rate-induced tipping (Fig. 13), we choose a segment consisting of the points between $t = 200$ and $t = 700$. This segment is in all probability too long, meaning that it also contains the transition itself, as opposed to only points prior to the transition. However, this is the inherent difficulty with rate-induced tipping; there is currently no way to analytically determine *when* the transition happens, and one largely has to guess. Based on Figs. 12 and 13, one could potentially conclude that the tipping point is found somewhere between $t = 400$ and $t = 600$, but this is pure guess work. For this reason, we have included points up until $t = 700$.

Given a set of measurements $Y_1, Y_2, \ldots, Y_N$, the sample variance is defined as

$$\sigma^2 = \frac{1}{N} \sum_{i=1}^{N} \left(Y_i - \overline{Y} \right)^2, \tag{19}$$
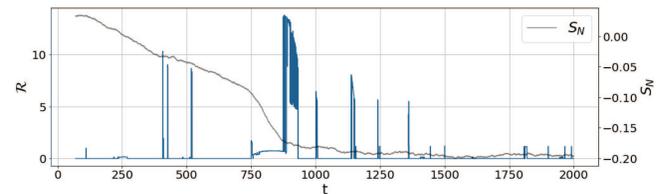

FIG. 16. Persistence of a time series undergoing rate-induced tipping, plotted as a function of time. The underlying series is the time series shown in Fig. 12. We see several high persistence values, corresponding with a high value for the order, $q + p$ (compare with Fig. 14), appearing before the potential tipping point around $t = 500$.
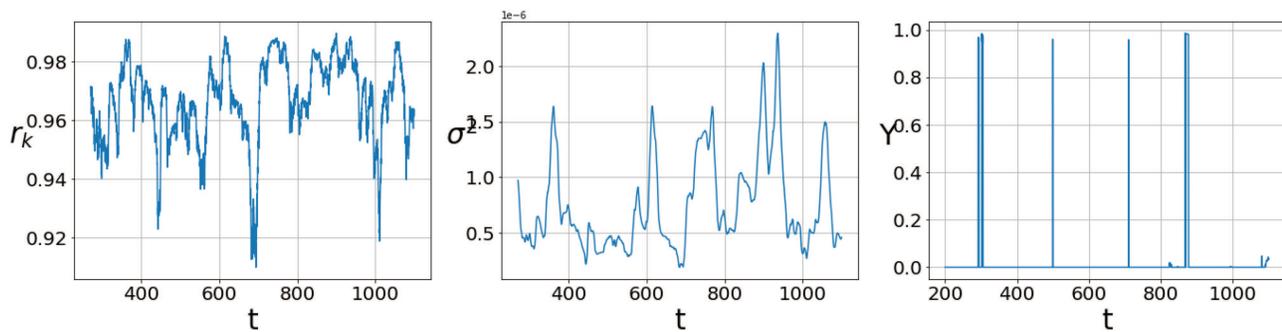
FIG. 17. Autocorrelation, variance, and Υ plotted as functions of time for a time series undergoing B-tipping. The increase in the variance as one approaches the tipping point is clear, while the increase in autocorrelation is less clear.

while the lag k autocorrelation is given by

$$r_k = \frac{1}{N\sigma^2} \sum_{i=1}^{N-k} \left(Y_i - \overline{Y}\right)\left(Y_{i+k} - \overline{Y}\right), \tag{20}$$

where $\overline{Y}$ denotes the sample mean of the series $Y_1, Y_2, \ldots, Y_N$ (see, for example, Chap. 2 of Box et al.[35]). Although time does not enter explicitly in the formulas, it is assumed that the measurements are taken at regular intervals.

When computing the variance and autocorrelation, it is essential that the signal is properly detrended; otherwise, any trend will immediately obscure the relevant dynamics. As for the Υ indicator, one generally employs a rolling window approach, with an appropriately chosen window length τ. Lenton et al.[33] demonstrated that detrending can be done within each time window, as opposed to on the whole time series at once, without significantly changing the result. We have chosen this same approach, using linear detrending, as opposed to quadratic or higher order detrending methods, to remove the trend. The window length τ was set to 350 points, corresponding to 70 years.

Figures 17 and 18 show the autocorrelation, variance, and Υ plotted as functions of time. The peaks in Υ preceding the transition are clear, as is the increase in variance and autocorrelation, at least

in the case of R-tipping, provided the tipping point is approximately at $t = 450$. For B-tipping, there appears to be a clear increase in the variance preceding the tipping point, provided the tipping point happens around $t = 850$ (see Fig. 4 for comparison). The expected increase in autocorrelation is, however, less clear.

It is possible that the high degree of autocorrelation in the three-box model, as observed in Figs. 17 and 18, is correlated to the frequent failure of the ARMA(1,0) model, whereby failure we mean that the autoregressive coefficient, sometimes referred to as the AR1 coefficient, violates the stationarity condition, resulting in ARMA(1,0) being excluded as a possible candidate model.

As already noted, the upper equilibrium branch does not lose stability due to a saddle-node bifurcation, but rather loses stability due to a sub-critical Hopf bifurcation. It is possible that classical indicators are struggling to pick up on this. Furthermore, the noise amplitude is kept low to avoid noise-induced tipping, which might make it difficult for the indicators to pick up on changes in the dynamics.

The autocorrelation and variance of a time series can increase for reasons that have nothing to do with an approaching tipping point. Hence, we wish to see how the Υ indicator responds to colored noise, whose variance and autocorrelation increases with time
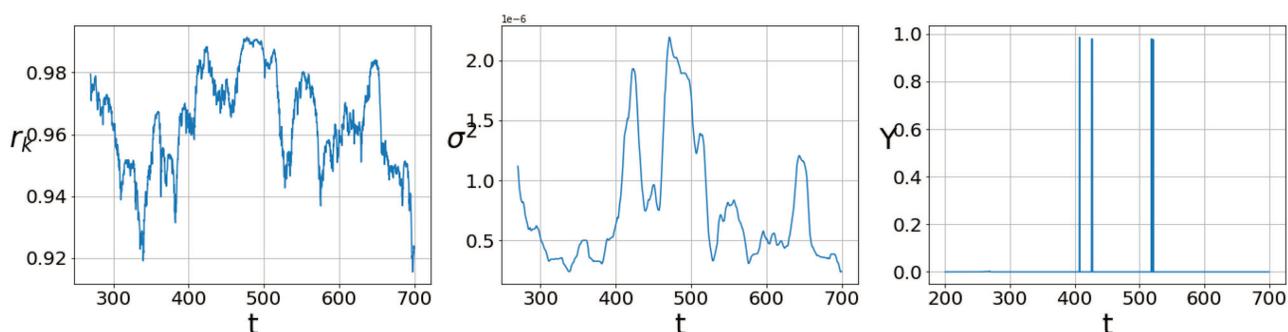

FIG. 18. Autocorrelation, variance, and Υ plotted as functions of time for a time series undergoing R-tipping. Assuming that the tipping point is around t = 450, one can clearly see an increase in both autocorrelation and variance prior to the tipping point.
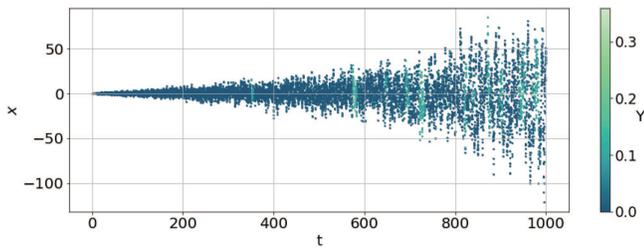
FIG. 19. Time series with colored noise but no tipping points, color coded according to the value of Υ.

t. To this end, we construct an artificial time series of the form

$$\frac{dx}{dt} = -5x + \xi(t), \tag{21}$$

where $\xi(t)$ is the autocorrelated colored noise. $\xi(t)$ is in effect modeled as an ARMA(1,0) process whose AR1 coefficient increases linearly in time. In addition, the variance of this process also increases linearly in time. This is equivalent to the example presented in Boers.[24] Applying the Υ indicator to this time series yields the result shown in Fig. 19. Figure 20 shows a comparison between the autocorrelation, variance, and value of Υ for the same time series. All three indicators show a dramatic increase despite there being no approaching tipping point. However, looking at the plot of the time series when color coded according to the values of p and q, Fig. 21, a curious pattern emerges: the increase in Υ is largely associated with an increased p value. Looking at Fig. 22, the trend becomes even clearer: here, we have computed the rolling average of the p and q values with a window length of 50 points corresponding to 25 non-dimensional time units. We see that while the average value of q goes toward zero for large t, the average value of p settles around one. The general trend is independent of the choice of window length, provided the window length is between 30 and 300 points.

This behavior is unlike what was observed for the three-box model. The high values of Υ were associated with a high value of q. We, thus, argue that high values of q were associated with increased
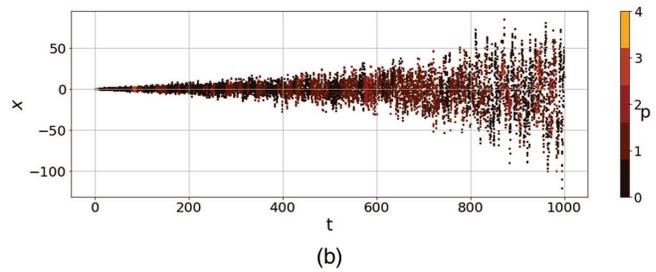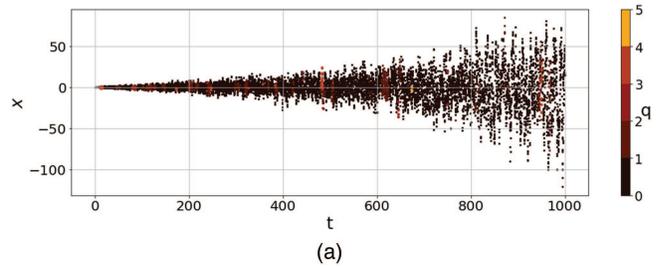

FIG. 21. Time series with colored noise and no tipping points, corresponding to equation (21), color coded according to the value of (a) q and (b) p.

instability, while high values of p were more indicative of the system following a moving equilibrium.

Thus, one would, through the distinction between q and p values, potentially have a way of distinguishing the effect of colored noise from real early-warning signals. However, it is conceivable that the result for the artificial colored noise time series is a consequence of how we have constructed the colored noise; therefore, further studies on this are warranted.

Finally, we note that the constructed colored noise time series is a very artificial example of colored noise, as the noise amplitude increases by a probably unrealistic amount, and when applied to any reasonable time series, it would obscure the dynamics altogether. This is to say that although we can likely assume that the noise in real-world data is autocorrelated, it will be much more subtle and not result in equally high values of Υ.
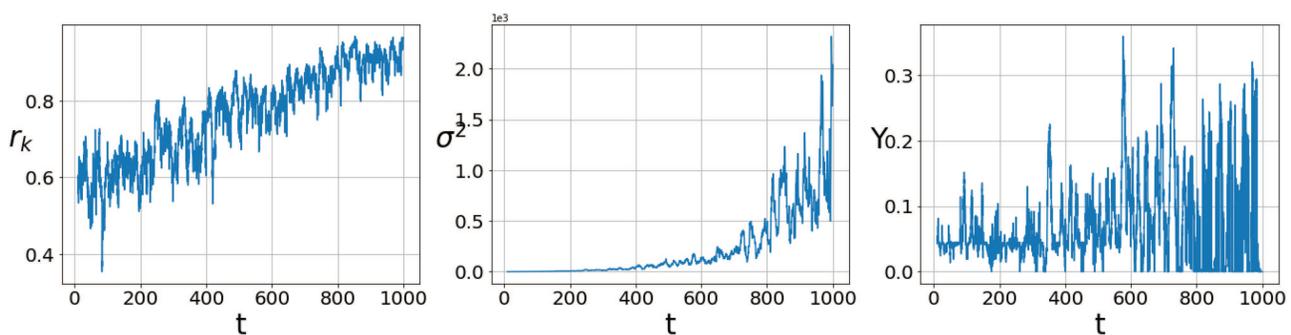

FIG. 20. Autocorrelation, variance, and Υ plotted as functions of time for a time series with colored noise but no tipping points. All three indicators show a dramatic increase, falsely suggesting an upcoming tipping point.
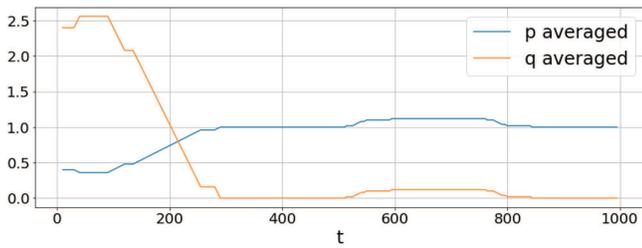
FIG. 22. The values of p and q for the colored noise time series, averaged with a window length of 50 points, corresponding to 25 non-dimensional time units.

FIG. 24. Time series of monthly density changes for abrupt $4 \times CO_2$, color coded according to the value of Υ. The window length is 250 points, corresponding to exactly 20 years. The dashed line indicates the point when the CO_2 concentration abruptly changes.

V. APPLICATION TO SIMULATION DATA FROM CESM2

So far, we have only applied the dynamic stability indicator to data from a very simplified model. The actual ocean has many more degrees of freedom, and the response could be quite different. Nevertheless, it is of interest to see how the indicator responds when applied to such a system. To this end, we employ data from the earth systems model CESM2 under two climate scenarios: one in which the atmospheric CO_2 concentration is abruptly doubled and another in which it is abruptly quadrupled. Both simulations were initialized using a pre-industrial control run (*piControl*) and then run for 500 years. The CO_2 was then increased at $t = 6000$ months. The data were saved at monthly intervals, and the seasonal cycle was removed prior to the analysis. Such an abrupt change in CO_2 represents an extreme forcing and contrasts with the ramped-up hosing employed with the idealized model. However, the oceanic response is not instantaneous, but requires two to three decades for freshwater to circulate in the model's sub-polar gyre.[27] We consider this more hereafter.

A. Abrupt $4 \times CO_2$

The time series of a monthly-mean density difference, $\delta\rho$, and AMOC strength, ψ_{AMOC}, are shown in Fig. 23 for the case of abrupt $4 \times CO_2$. The density difference, a measure dynamically linked to the AMOC strength (Madan *et al.*[27]), is calculated from the difference in surface densities averaged in boxes to the north and south of the North Atlantic Current. The surface density is calculated using the thermodynamic equation of state of seawater as per the UNESCO 1983 Report.[36] The AMOC strength is calculated
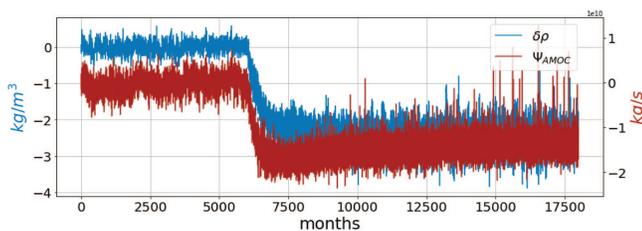
as the monthly maxima of meridional overturning stream function between $20°N$ and $60°N$ and below 450 m depth.

Shortly after the quadrupling of CO_2, there is an abrupt transition followed by a dramatic increase in the variance. We will apply the indicator to the density difference time series, although one could of course apply the same analysis to the AMOC strength.

We choose a window length of 250 data points, corresponding to exactly 20 years of monthly data. Figure 24 shows the density difference, $\delta\rho$, color coded according to the values of Υ. We only display the part of the time series close to the transition, as this is of primary interest. The point at which the CO_2 concentration is abruptly increased, at $t = 6000$ months, is indicated by a dashed line.

The increase in Υ during the early part of the AMOC weakening process is apparent. Note, in particular, the three sharp peaks shortly after time t = 6000. Figure 25 again shows the time series,

(a)

(b)

FIG. 25. Time series of monthly density changes for abrupt $4 \times CO_2$, color coded according to the value of (a) q and (b) p. The values for q and p are also plotted as functions of time in (a) and (b), respectively.

FIG. 23. CESM2 model with abrupt $4 \times CO_2$, where the monthly density difference (blue) is plotted together with the maximum AMOC flow strength (red). Note that the CO_2 was increased at t = 6000 months.
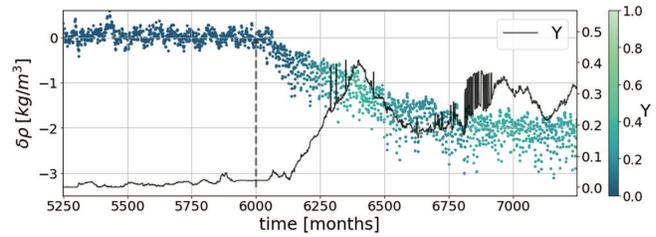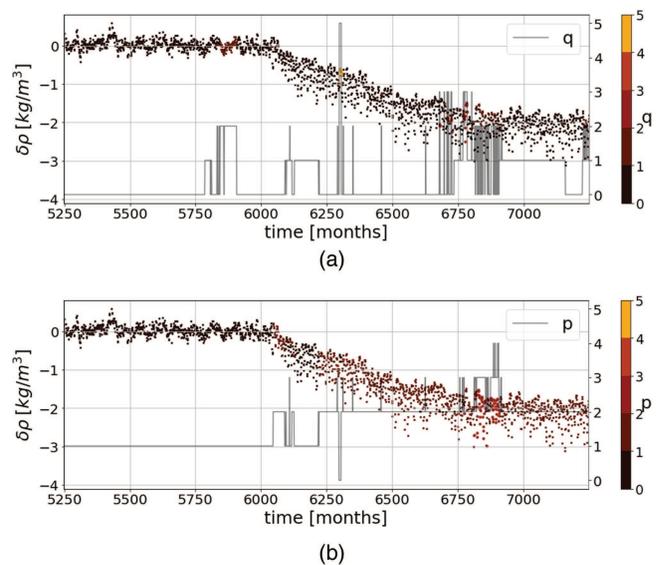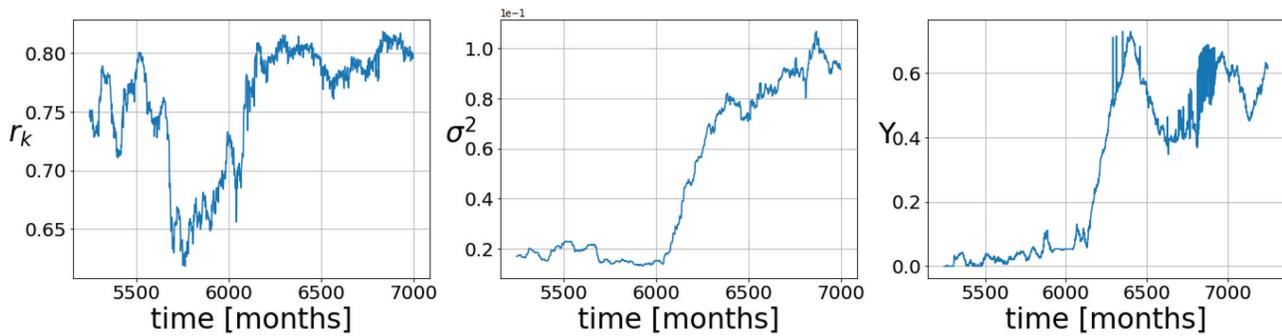
FIG. 26. Autocorrelation, variance, and Υ plotted as functions of time for the case of abrupt $4 \times CO_2$.

now color coded according to the values of q and p. The latter are also plotted for further clarification. From this plot, it becomes clear that the most common fit prior to the transition is the ARMA(1,0) process, which aligns with the observations of Faranda *et al.*[10] After the weakening phase, the value of p is generally an order higher, presumably related to the dramatic increase in the variance. The three sharp peaks in the plot of Υ appearing around time $t = 6300$ correspond to high values of q. The gradual increase in Υ preceding these peaks is presumably due to the increase in the persistence (not shown). The q component exhibits peaks prior to $t = 6000$ when the forcing is applied, and these are reflected in small peaks in Υ. These are obviously not connected to the AMOC weakening. Following the initial weakening phase, the value for Υ remains high, probably a result of the increase in the p value. However, the values of Υ do not go above 0.4, which is considerably smaller than the values found for the three-box model. In addition, from our previous discussion on the response of the Υ indicator to colored noise, it is conceivable that the increase in Υ observed from the CESM2 data is primarily caused by changes in the noise amplitude and not as a consequence of inherent instability of the underlying dynamics.

Furthermore, we note that, although the result is not explicitly shown, for the CESM2 data, ΔBIC_1 is always smaller than ΔBIC_0, and the ΔBIC_1 values are at no point negative, implying that the autoregressive coefficient in the ARMA(1,0) model always satisfy the stationarity constraints. This differs from what was observed in the three-box model and is presumably related to the difference in the observed Υ values.

However, we emphasize that it is not clear if one, in actuality, can compare values of Υ between datasets. For the autocorrelation and the variance, it is typically assumed that it is the change *within* the dataset that is significant, rather than the absolute numerical values.

For completeness, we have included a comparison between Υ and two other statistical early-warning indicators, namely, autocorrelation and variance. This is shown in Fig. 26. In all cases, the window length is 250 points, corresponding to approximately 20 years. All three indicators show a clear increase shortly after time $t = 6000$.

B. Abrupt $2 \times CO_2$

The time series of the monthly density difference, $\delta\rho$, and AMOC strength, ψ_{AMOC}, in the case of abrupt $2 \times CO_2$ is shown in Fig. 27. Again, we only apply the indicator to the density difference data and choose the same window length as in the case of abrupt $4 \times CO_2$. Figure 28 shows an excerpt of the density difference time series close to the initial weakening, as well as a plot of the Υ values. A weakening is clearly seen in the model's own AMOC measure and is also accurately captured with the measure based on the density difference across the Gulf Stream (Fig. 27).

The first thing to note is how small the Υ values are compared to what we have seen previously—on the order of 10^{-2}. It should, however, be noted that the ΔBIC values are well above the significance threshold.[29] Figure 29 shows the density difference time series color coded according to the value of q and p. From this, we again

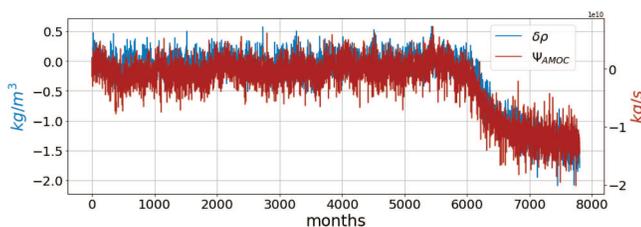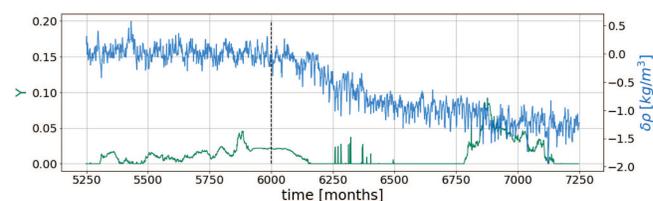**FIG. 27.** CESM2 model with abrupt $2 \times CO_2$, where the monthly density difference (blue) is plotted together with the maximum AMOC flow strength (red).

FIG. 28. Monthly density changes, $\delta\rho$, for abrupt $2 \times CO_2$ (blue) and the value of Υ (green) plotted as functions of time. The dashed line indicates the point when the CO_2 concentration abruptly changes.
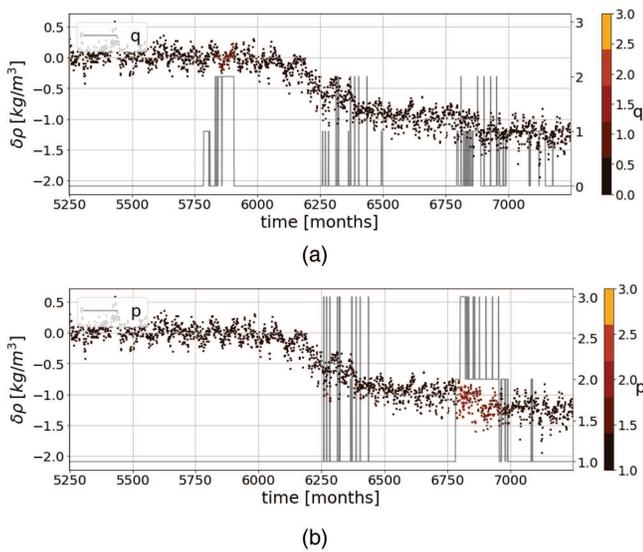
FIG. 29. Time series of monthly density changes for abrupt $2 \times CO_2$, color coded according to the value of (a) q and (b) p. The values for q and p are also plotted as functions of time in (a) and (b), respectively.

see that prior to the increase in CO_2, the most common fit is the ARMA(1,0) process, while after the initial weakening phase, the p values show a clear increase. The q value, on the other hand, does not exceed 2, indicating a very low degree of memory in the noise term. Since we have by now clearly demonstrated a correlation with the value of Υ and the value of q, this should provide an explanation as to why we see such low values of Υ. From this analysis, one would conclude that the system does not appear to be approaching a tipping point. Indeed, the measure suggests that the weakening in the overturning in this case with reduced forcing is not associated with a loss of dynamical stability. Once more, we have, as shown in Fig. 30, included a comparison with other early-warning indicators. The autocorrelation and variance show a dramatic increase around time t = 6000, which corresponds to the appearance of the cluster of sharp peaks in the time series plot for Υ.

VI. DISCUSSION

In summary, we analyzed an indicator for dynamical stability based on ARMA modeling as a way to detect transitions in complex
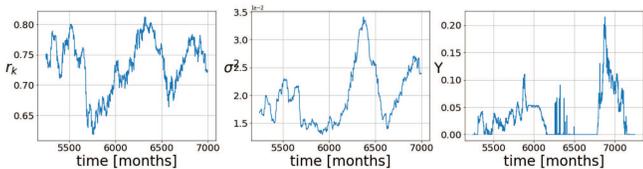

FIG. 30. Autocorrelation, variance, and Υ plotted as functions of time for the case of abrupt $2 \times CO_2$.

systems. A detected need for higher order terms in the ARMA model fitted to moving windows of a time series is related to diverging memory properties, which are expected to arise when approaching a transition to a new equilibrium state. The rationale behind this indicator is that it uses a broad family of linear statistical models that can be fitted even on short time series and which have proven their utility in many contexts (see Brockwell and Davis[28]). That the underlying models do not require long time series is an advantage when employing a sliding window approach on limited data sets. The method generalizes classical metrics of instability and allows one to extract more global dynamical information from the time series data.

The indicator was tested on time series data from a three-box model of the AMOC, where three categories of critical transitions, namely, B-, N-, and R-tipping, were explored. In all cases, the transition is identified by the indicator, albeit it is not always easy to interpret the signal. In the rate-induced tipping scenario, a comparison between the avoided tipping and the tipping cases shows a response of the indicator prior to the transition only in the tipping case, although the time series are nearly identical at this stage. The indicator also successfully identifies the unstable limit cycle when returning to the upper equilibrium branch. We similarly see fairly clear signals in the bifurcation-induced tipping scenario prior to the transition. For the case of noise-induced tipping, the signal is less clear, obscured by the high amplitude noise. However, when going from the lower to upper equilibrium branch, the indicator signals an increased degree of instability in accordance with the presence of the unstable limit cycle.

The primary drawback of the Υ indicator is that it is computationally quite expensive, at least compared to the autocorrelation and variance, and that, due to its complexity, the results can be harder to interpret. We, therefore, suggest that the indicator should be applied with care and preferably in combinations with other measures of instability, such as the increase in the order, $p + q$, and the persistence. Although the current scaling with τ, see equation (3), seems to yield reasonable results, it is certainly possible that another scaling would be preferred. It is also possible that this is problem-dependent. This uncertainty regarding the correct scaling is certainly a drawback, but we argue that this problem can largely be circumvented by including an examination of the persistence and order values. However, it would still be advantageous to have an indicator whose values were to have a clear meaning in terms of the stability of the system, and it is not clear if the Υ indicator as it stands achieves this, partly due to the aforementioned issue with the choice of the correct scaling. Although we have attempted to make some comparison to other early-warning indicators, such as the increase in autocorrelation and variance, we are not claiming that the Υ indicator is in any way better than these other indicators, rather that it can act as a complementary approach, as it can allow one to extract more information from time series data. For example, we have suggested that it might be helpful in identifying the effects of colored noise, something the other indicators struggle with.

Furthermore, we note that it is conceivable that one would wish to exclude white noise and pure moving-average, MA(1), processes when doing the fitting, as was done in the earlier studies by Faranda et al.[10] In such a scenario, the modified definition of the Υ

indicator would of course no longer be valid, as the ARMA(0,0) process is excluded, and, therefore, cannot be used as a base model. In this case, one might argue that the points where Δ_1BIC are negative should either be ignored completely or one should assume that the best fit is, in fact, the ARMA(1,0) process and the algorithm is being too strict in its enforcement of the auxiliary conditions on the fitting parameters. This would of course lead to different results than what has been presented here and is an option worth considering.

When considering a full complexity AMOC model as arising from a global climate model (CESM2), many more degrees of freedom are involved. This has two consequences: first, the pure categories of tipping cannot really be expected anymore, and second, the tipping behavior might disappear altogether as the added degrees of freedom may stabilize the system.

When applied to the CESM2 data, the results were mixed. The measure exhibited a significant increase in Υ under the more severe $4 \times CO_2$ forcing but much less variability with the weaker $2 \times CO_2$ forcing. Hence, the measure only registers larger changes in AMOC as associated with dynamically unstable behavior. Indeed, it is possible that the model AMOC experiences a continuously shifting steady state, rather than making a transition between two distinct states as in low dimensional models. The results from the doubling CO_2 experiment seem to support this hypothesis. Other members of the CMIP6 ensemble exhibit very different AMOC weakening from the same forcing, with some declining by only 15% and others falling by 80%,[27] and this suggests a continuum of different responses.

While the results for $4 \times CO_2$ suggest a loss of dynamical stability during the AMOC weakening phase, concluding on the tipping behavior would require a more in depth analysis along the lines done in Hawkins *et al.*;[23] in this paper, the bi-stability is clearly demonstrated by exploring a range of hosing experiments. Although we are confident that the Υ indicator can be used to assess the stability of such complex systems, as was already demonstrated in previous works by Nevo *et al.*,[12] concluding on the ability to detect critical transitions would require a full analysis of the hysteresis behavior of the system.[23]

ACKNOWLEDGMENTS

AUTHOR DECLARATIONS

Conflict of Interest

The authors have no conflicts to disclose.

Author Contributions

Marie Rodal: Data curation (equal); Formal analysis (equal); Methodology (equal); Software (equal); Validation (equal); Visualization (equal); Writing – original draft (equal); Writing – review & editing (equal). **Sebastian Krumscheid:** Conceptualization (equal); Methodology (equal); Supervision (equal); Writing – original draft (equal); Writing – review & editing (equal). **Gaurav Madan:** Data curation (equal); Writing – original draft (equal); Writing – review & editing (equal). **Joseph Henry LaCasce:** Data curation (equal); Supervision (equal); Writing – original draft (equal); Writing – review & editing (equal). **Nikki Vercauteren:** Conceptualization (equal); Funding acquisition (equal); Methodology (equal); Project administration (equal); Supervision (equal); Writing – original draft (equal); Writing – review & editing (equal).

DATA AVAILABILITY

The data that support the findings of this study are available from the corresponding author upon reasonable request. The code used for the numerical analysis will be made available in a GitHub folder (https://github.com/MarieRodal).

REFERENCES

[1] T. M. Lenton, "Environmental tipping points," Annu. Rev. Environ. Resour. **38**, 1–29 (2013).

[2] P. Ashwin, S. Wieczorek, R. Vitolo, and P. Cox, "Tipping points in open systems: Bifurcation, noise-induced and rate-dependent examples in the climate system," Philos. Trans. R. Soc. A **370**, 1166–1184 (2012).

[3] M. Scheffer, E. H. Van Nes, M. Holmgren, and T. Hughes, "Pulse-driven loss of top-down control: The critical-rate hypothesis," Ecosystems **11**, 226–237 (2008).

[4] S. Wieczorek, P. Ashhwin, C. Luke, and P. M. Cox, "Excitability in ramped systems: The compost-bomb instability," Philos. Trans. R. Soc. A **467**, 2733 (2011).

[5] P. E. O'Keeffe and S. Wieczorek, "Tipping phenomena and points of no return in ecosystems: Beyond classical bifurcations," SIAM J. Appl. Dyn. Syst. **19**, 2371–2402 (2020).

[6] S. Wieczorek and C. Perrymann, "Adapting to a changing environment: Non-obvious thresholds in multi-scale systems," Proc. R. Soc. A **470**, 20140226 (2014).

[7] P. Ashwin, C. Perrymann, and S. Wieczorek, "Parameter shifts for nonautonomous systems in low dimension: Bifurcation- and rate-induced tipping," Nonlinearity **30**, 2185–2210 (2017).

[8] A. Vanselow, S. Wieczorek, and U. Feudel, "When very slow is too fast-collapse of a predator-prey system," J. Theor. Biol. **479**, 64–72 (2019).

[9] P. Ritchie and J. Sieber, "Early-warning indicators for rate-induced tipping," Chaos **26**, 093116 (2016).

[10] D. Faranda, F. M. E. Pons, E. Giachino, S. Vaienti, and B. Dubrulle, "Early warnings indicators of financial crises via auto regressive moving average models," Commun. Nonlinear Sci. Numer. Simul. **29**, 233–239 (2015).

[11] D. Faranda, B. Dubrulle, and F. M. E. Pons, "Statistical early-warning indicators based on autoregressive moving-average models," J. Phys. A: Math. Theor. **47**, 252001 (2014).

[12] G. Nevo, N. Vercauteren, A. Kaiser, B. Dubrulle, and D. Faranda, "Statistical-mechanical approach to study the hydrodynamic stability of the stably stratified atmospheric boundary layer," Phys. Rev. Fluids **2**, 084603 (2017).

[13] A. Kaiser, D. Faranda, S. Krumscheid, D. Belusic, and N. Vercauteren, "Detecting regime transitions of the nocturnal and polar near-surface temperature inversion," J. Atmos. Sci. **77**, 2921–2940 (2020).

[14] D. Faranda and D. Defrance, "A wavelet-based approach to detect climate change on the coherent and turbulent component of the atmospheric circulation," Earth Syst. Dyn. **7**, 517–523 (2016).

[15] H. Alkhayuon, P. Ashwin, L. C. Jackson, C. Quinn, and R. A. Wood, "Basin bifurcations, oscillatory instability and rate-induced thresholds for Atlantic

meridional overturning circulation in a global oceanic box model," Proc. R. Soc. A **475**, 20190051 (2019).

[16]R. A. Wood, J. M. Rodriguez, R. S. Smith, L. C. Jackson, and E. Hawkins, "Observable, low-order dynamical controls on thresholds of the Atlantic meridional overturning circulation," Clim. Dyn. **53**, 6815–6834 (2019).

[17]*IPCC 2021: Climate Change 2021: The Physical Science Basis. Contribution of Working Group I To the Sixth Assessment Report of the Intergovernmental Panel on Climate Change*, edited by V. Masson-Delmotte, P. Zhai, A. Pirani, S. Connors, C. Péan, S. Berger, N. Caud, Y. Chen, L. Goldfarb, M. Gomis, M. Huang, K. Leitzell, E. Lonnoy, J. Matthews, T. Maycock, T. Waterfield, O. Yelekçi, R. Yu, and B. Zhou (Cambridge University Press, 2021).

[18]W. Weijer, W. Cheng, S. S. Drijfhout, A. Federov, A. Hu, and L. C. Jackson, "Stability of the Atlantic meridional overturning circulation: A review and synthesis," J. Geophys. Res.: Oceans **124**, 5336–5375, https://doi.org/10.1029/2019JC015083 (2019).

[19]M. Hofmann and S. Rahmsdorf, "On the stability of the Atlantic meridional overturning circulation," Proc. Natl. Acad. Sci. U.S.A. **106**, 20584–20589 (2009).

[20]W. Liu, S.-P. Xie, Z. Liu, and J. Zhu, "Overlooked possibility of a collapsed Atlantic meridional overturning circulation in warming climate," Sci. Adv. **3**, e1601666 (2017).

[21]S. E. Huisman, M. den Toom, H. A. Dijkstra, and S. Drijfhout, "An indicator of the multiple equilibria regime of the Atlantic meridional overturning circulation," J. Phys. Oceanogr. **40**, 551–567 (2010).

[22]W. Liu, Z. Liu, and E. C. Brady, "Why is the AMOC monostable in coupled general circulation models?," J. Clim. **27**, 2427–2443 (2014).

[23]E. Hawkins, R. Smith, L. Allison, J. Gregory, T. Woollings, H. Pohlmann, and B. de Cuevas, "Bistability of the Atlantic overturning circulation in a global climate model and links to ocean freshwater transport," Geophys. Res. Lett. **38**, L10605, https://doi.org/10.1029/2011GL047208 (2011).

[24]N. Boers, "Observation-based early-warning signals for a collapse of the Atlantic meridional overturning circulation," Nat. Clim. Change **11**, 680–688 (2021).

[25]J. Lohman and P. D. Ditlevsen, "Risk of tipping the overturning circulation due to increasing rates of ice melt," Proc. Natl. Acad. Sci. U.S.A. **118**, e2017989118 (2021).

[26]G. Danabasoglu, "NCAR CESM2 model output prepared for CMIP6 CMIP," (2019). https://doi.org/10.22033/ESGF/CMIP6.2185.

[27]G. Madan, A. Gjermundsen, S. Iversen, and J. H. LaCasce, "Weakening of the Atlantic meridional overturning circulation under extreme climate change," (unpublished) (2022).

[28]P. J. Brockwell and R. A. Davis, *Introduction to Time Series and Forecasting*, 2nd ed. (Springer, 2002).

[29]K. J. Preacher and E. C. Merkle, "The problem of model selection uncertainty in structural equation modeling," Psychol. Methods **17**, 1–14 (2012).

[30]R. J. Hyndman and Y. Khandakar, "Automatic time series forecasting: The forecast package for R," J. Stat. Softw. **27**, 1–22 (2008).

[31]J. M. T. Thompson and J. Sieber, "Climate tipping as a noisy bifurcation: A predictive technique," IMA J. Appl. Math. **76**, 27–46 (2011).

[32]D. Roche, D. Paillard, T. Caley, and C. Waelbroeck, "LGM hosing approach to Heinrich Event 1: Results and perspectives from data-model integration using water isotopes," Quat. Sci. Rev. **106**, 247–261 (2014).

[33]T. M. Lenton, V. N. Livina, V. D. Dakos, E. H. van Nes, and M. Scheffer, "Early warning of climate tipping points from critical slowing down: Comparing methods to improve robustness," Philos. Trans. R. Soc. A **370**, 1185–1204 (2012).

[34]V. Dakos, S. R. Carpenter, W. A. Brock, A. M. Ellison, V. Guttal, A. R. Ives, S. Kefi, V. Livina, D. A. Seekell, E. H. van Nes, and M. Scheffer, "Methods for detecting early warnings of critical transitions in time series illustrated using simulated ecological data," PLoS One **7**, e41010 (2012).

[35]G. E. Box, G. M. Jenkins, and G. C. Reinsel, *Time Series Analysis: Forecasting and Control*, 4th ed. (Wiley & Sons, Inc., 2008).

[36]N. P. Fofonoff and R. Millard, Jr., *Algorithms for Computation of Fundamental Properties of Seawater,* UNESCO Technical Papers in Marine Sciences 44 (UNESCO, Paris, 1983).